Sensors & Transducers, Vol. 169, Issue 4, April 2014, pp. 241-249

Sensors & Transducers

Decoupling Research on Flexible Tactile Sensors Interfered by White Gaussian Noise Using Improved Radical Basis Function Neural Network

[1, 2, 3] Feilu Wang, [1] Hongqing Pan, [1] Yubing Wang, [1] Ming Zhu, [1] Yong Yu, [1] Junxiang Ding, [1, 3, *] Feng Shuang

[1] Institute of Intelligent Machines, Chinese Academy of Sciences, Hefei, 230031, China
[2] School of Electronics and Information Engineering, Anhui Jianzhu University, Hefei, 230601, China
[3] Department of Automation, University of Science and Technology of China, Hefei, 230027, China
[*] E-mail: fshuang@iim.ac.cn

Received: 18 April 2014 /Accepted: 28 April 2014 /Published: 30 April 2014

Abstract: Research on tactile sensors to enhance their flexibility and ability of multi-dimensional information detection is a key issue to develop humanoid robots. In view of that the tactile sensor is often affected by noise, this paper adds different white Gaussian noises (WGN) into the ideal model of flexible tactile sensors based on conductive rubber purposely, then improves the standard radial basis function neural network (RNFNN) to deal with the noises. The modified RBFNN is applied to approximate and decouple the mapping relationship between row-column resistance with WGNs and three-dimensional deformation. Numerical experiments demonstrate that the decoupling result of the deformation for the sensor is quite good. The results show that the improved RBFNN which doesn't rely on the mathematical model of the system has good anti-noise ability and robustness. *Copyright © 2014 IFSA Publishing, S. L.*

Keywords: White Gaussian noise, Decouple, Conductive rubber, Flexible tactile sensor, Radical basis function neural network.

1. Introduction

With the development of robot technology, the tactile sensor as an important part of robot perception system has been widely concerned. Tactile sensors can help the robot to feel and recognize objects, and to complete a variety of complex tasks. At present, most of the design principle for the sensitive element of the tactile sensor is mainly based on piezoresistive, capacitive, piezoelectric, PDMS, optical fiber and silicon etching technology etc. [1-5]. All of that have achieved a series of research results. Especially, Zhenan Bao, *et al.* [3] proposed a highly sensitive flexible pressure sensor with microstructured rubber dielectric layers, and the sensor can be inexpensively fabricated over large areas. The key component of that material design is the microstructuring of thin films of the dielectric elastomer polydimethylsiloxane (PDMS). As the robot skin, the tactile sensor is required to detect three-dimensional (3-d) information and has good flexibility. As a flexible material, the conductive rubber has excellent piezoresistive effect and flexibility, which makes it an ideal material to develop tactile sensors. Recent years, the conductive rubber gets the wide attention of researchers [6-8]. In this area, Tao Liu [8] proposed a touch sensor covered by conductive

rubber, and the bottom of the sensor lays comb detecting circuit, however, due to its isolated cell structure, it cannot be used for large area touch detection.

In practical application, the 3-d deformation and 3-d force exerted on the tactile sensor are difficult to detect, so the decoupling technology for the 3-d information become a very important part in the design of flexible tactile sensors system. Kim, *et al.* [9] designed a bio-mimetic tactile sensor that can measure three components forces. Nowadays, researchers pay more attention to the decoupling algorithms of the tactile sensor based on conductive rubber. Some researchers use intelligent algorithms to decouple the multi-dimensional information for tactile sensors under ideal conditions [10-13]. Ding, *et al.* [11] presented a decoupling algorithm based on homotopy theory. Wang, *et al.* [12-13] decoupled the mapping relationship between 3-d information of the tactile sensor based on artificial neural network methods under the ideal conditions.

This paper proposes adding different noises into the ideal flexible tactile sensor model purposely to simulate the real situation of the tactile sensor and improves the RBFNN. In Sec. 2, the properties of the flexible tactile sensor, the mathematical model of the sensor, and Gaussian noise are introduced. Sec. 3 shows the structure of the improved RBFNN. In Sec. 4, the modified RBFNN algorithm is applied to decouple the mapping relationship from resistance to 3-d deformation of the flexible tactile sensor interfered by different noises.

2. A Flexible Tactile Sensor Based on Conductive Rubber

2.1. Properties of Conductive Rubbers

The conductive rubber is composed of conductive powers such as carbon black and metal, which are mixed and dispersed in silicone rubber material. When the conductive rubber is subjected to external force or load, the resistance value of its own will be changed accordingly. That characteristic is the force-sensitive property of the conductive rubber. The force-sensitive conductive rubber is a novel kind of sensitive material. It not only has good mechanical properties, but also has good flexibility, easy molding, and simple making technology, etc.

In this paper, the flexible tactile sensor for our experiments is designed based on the force-sensitive conductive rubber [14]. The related properties of force-sensitive conductive rubber under ideal conditions are as follows [7]:

1) The rubber material is continuous;

2) The rubber material is homogeneous, each part of the rubber has the same elastic;

3) The rubber is an ideal elastic body, with a small deformation, the relation (shown in Fig. 1) between deformation and external force satisfies the generalized Hooke law.

$$\begin{aligned} F_x &= k_x \times \Delta x \\ F_y &= k_y \times \Delta y \\ F_z &= k_z \times \Delta z \end{aligned} \tag{1}$$

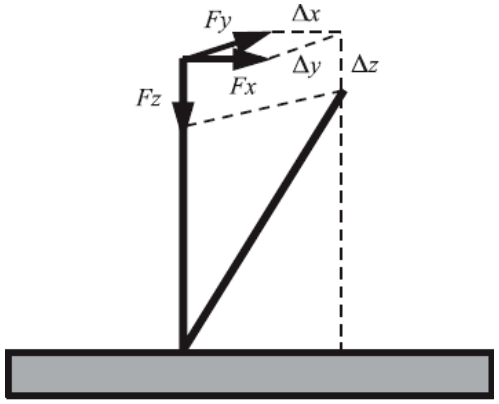

Fig. 1. The relation between deformation and external force.

4) On the premise of cross-sectional area is known, the resistance value R of the rubber is proportional to the length L of its own: $R = g \times L$.

2.2. The Detection Principle of the Tactile Sensor

As the conductivity of the rubber, there exist resistances between electrodes on different layers of the tactile sensor. The resistance between an electrode on the upper layer and another electrode on the lower layer is called "node resistance" (shown in Fig. 2). It is assumed that when a force or load is applied on the upper layer of the sensor, the electrodes on the lower layer are not deformed. According to the ideal characteristic of a conductive rubber, the resistance between an upper electrode and a lower electrode is proportional to the distance of those two electrodes.

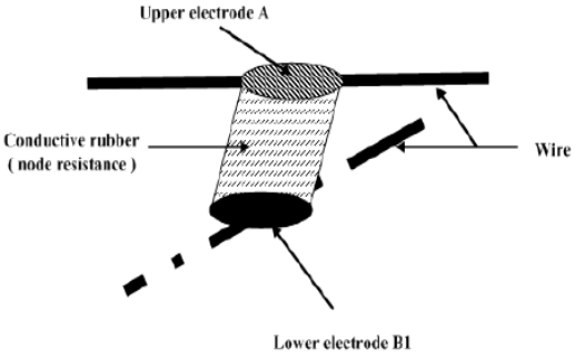

Fig. 2. Node resistance.

In Fig. 2, when there is no load or external force applied on the tactile sensor, the node resistance between the electrode A on the upper layer and the electrode B1 on the lower layer is:

$$R_{AB_1} = g \times |AB_1| = g \times \sqrt{(x_A - x_{B_1})^2 + (y_A - y_{B_1})^2 + (z_A - z_{B_1})^2}, \quad (2)$$

where g is the constant, usually g=100 Ω/mm.

When a force applied on the upper surface of the sensor, the position of the electrodes on the upper layer of the conductive rubber would be changed and the upper surface of the sensor would be deformed. It is supposed that the upper electrode A moved to A', so the node resistance between A' and B1 is:

$$R_{A'B_1} = g \times |A'B_1| = g \times \sqrt{(x_{A'} - x_{B_1})^2 + (y_{A'} - y_{B_1})^2 + (z_{A'} - z_{B_1})^2}$$
$$x_{A'} = x_A - \Delta x_A,\ y_{A'} = y_A - \Delta y_A,\ z_{A'} = z_A - \Delta z_A \quad (3)$$

When a force is applied on the upper surface of the flexible tactile sensor, the conductive rubber would be deformed. Thereby, the position of the internal electrodes of the sensor would be changed accordingly, that leads to the "node resistance" changed. So, we should deduce and decouple the deformation of the sensor from the changed resistance that can be detected by the external circuit firstly. Then the force information loaded on could be computed.

2.3. The Mathematical Model of the Flexible Tactile Sensor

In our experiment, the electrodes and wires are two layer distributed inside of the flexible sensor based on the conductive rubber [15]. The wires (shown in Fig. 2 and Fig. 3) on the upper layer are called "row-wire" and the wires on the lower layer are called "column-wire". The electrodes on the upper layer are connected horizontally by the "row-wire", while the electrodes on the lower layer are connected vertically by the "column-wire" (shown in Fig. 3). Electrodes are set on each wire embedded in the rubber, the resistance between each row-wire on the upper layer and the column-wire on the lower layer is called "row-column resistance" that can be regarded as equivalent parallel resistance of all the resistances of the electrodes on the two wires. The parallel resistance model for the flexible tactile senor based on conductive rubber is shown in Fig. 3. In the practical application, the number of electrodes and the array size of the sensor can be adjusted according to the scale and resolution of the flexible tactile sensor.

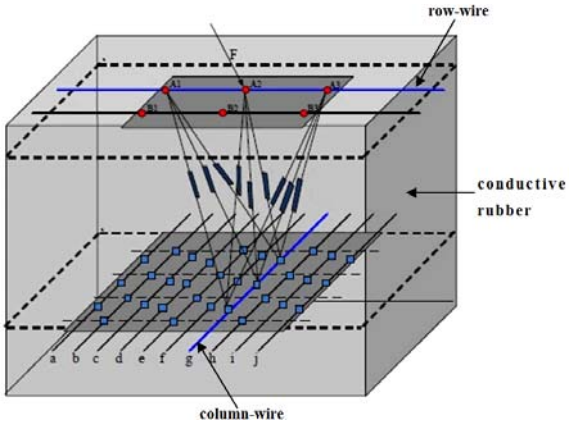

Fig. 3. The parallel resistance model.

The parallel row-column resistance between the m-th row-wire and the k-th column-wire can be expressed as follows.

$$R_{mk} = R_{m_1k_1} \,||\, R_{m_1k_2} \,||\, \ldots \,||\, R_{m_1k_M} \,||\, \ldots \,||\, R_{m_Nk_1} \,||\, R_{m_Nk_2} \,||\, \ldots \,||\, R_{m_Nk_M}, \quad (4)$$

$$g\left(\sum_{j=1}^{M}\sum_{i=1}^{N}\frac{1}{\sqrt{(x_i - x_{jk}^L)^2 + (y_i - x_{jk}^L)^2 (z_i - z_{jk}^L)^2}}\right)^{-1} = R_{mk}, k = 1,2,\ldots,3N \quad (5)$$
$$x_i = x_i^U - \Delta x_i,\ y_i = y_i^U - \Delta y_i,\ z_i = z_i^U - \Delta z_i$$

where N is the number of the electrodes on each row-wire, M is the number of the electrodes on each column-wire, i and j are the label of the electrodes on the m-th row-wire and the k-th column-wire separately, m and k are the label of the row-wire and the column-wire respectively; x_i^U, y_i^U and z_i^U represent the 3-d coordinate of the i-th electrode on the m-th row-wire when there is no force loaded on the sensor; Δx_i, Δy_i, and Δz_i represent the 3-d deformation accordingly; x_i, y_i, and z_i represent the 3-d coordinate of the i-th node on a row-wire under the 3-d force; x_{jk}^L, y_{jk}^L, z_{jk}^L denote the coordinate of the j-th electrode on the k-th column-wire, all of them are already known when the sensor is designed. In the simulation, m=1, 2, …, 8, k=18, N=6, M=3.

Actually, Eq. (5) is an equation set that contains 3N variables which denote the 3-d deformation of N electrodes. From the 3N equations, the 3N variable can be solved. Eq. (5) indicates that the row-column resistance R_{mk} only has connection with the coordinates and deformation of the N electrodes on the current row-wire. So, Eq. (5) can be described as Eq. (6). The row-column parallel resistance can be detected from the circuit, and the 3-d deformation of the N electrodes on each row-wire can be solved through Eq. (5).

$$R_{mk} = f(x_1, y_1, z_1, x_2, y_2, z_2, \ldots, x_N, y_N, z_N)$$
$$k = 1, 2, \ldots, 3N \tag{6}$$

The above formulas are proposed based on the ideal conditions of conductive rubber. In practical application, the sensor is often affected by the noise in the process of measuring the row-wire resistance through the external circuit, which also affects the accuracy of the tactile sensor model. Consequently, that will lead to a lot of errors in the decoupling procedure for the 3-d deformation or 3-d force information. So, we want to add some random noise into the ideal model of the sensor. In order to simulate the actual situation, we change the parallel resistances model into Eq. (7), in which, random White Gaussian Noise (WGN) is added to imitate the real situation of the sensor in practical application. After that, Eq. (7) is more close to the actual condition of the sensor. In the decoupling experiments, different extent WGNs are put into the model (such as 5 % White Gaussian Noise etc.) to explore the approximation error of the RBFNN. The WGN is adopted because in the actual system, the main noise source is the thermal noise, and the thermal noise is a typical WGN. The Gaussian noise is random noise.

$$g\left(\sum_{j=1}^{M}\sum_{i=1}^{N}\frac{1}{\sqrt{(x_i - x_{jk}^L)^2 + (y_i - x_{jk}^L)^2 (z_i - z_{jk}^L)^2}}\right)^{-1} + WGN$$
$$= R_{mk}, k = 1, 2, \ldots, 3N \tag{7}$$

Fig. 4 shows the row-column resistance when no noise added to the flexible tactile sensor, while Fig. 5 shows the row-column resistance when 5 % WGN added.

In this paper, the modified RBFNN is constructed, and it is used to approximate the mapping relation between 3-d deformation of the electrodes on the row-wire and row-column resistances for the tactile sensor interfered by WGNs.

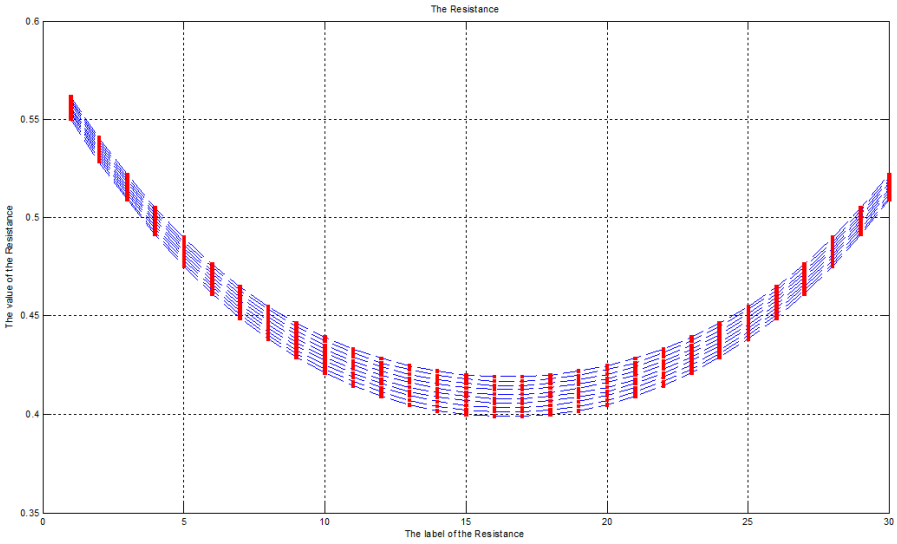

Fig. 4. The row-column resistance with no noise.

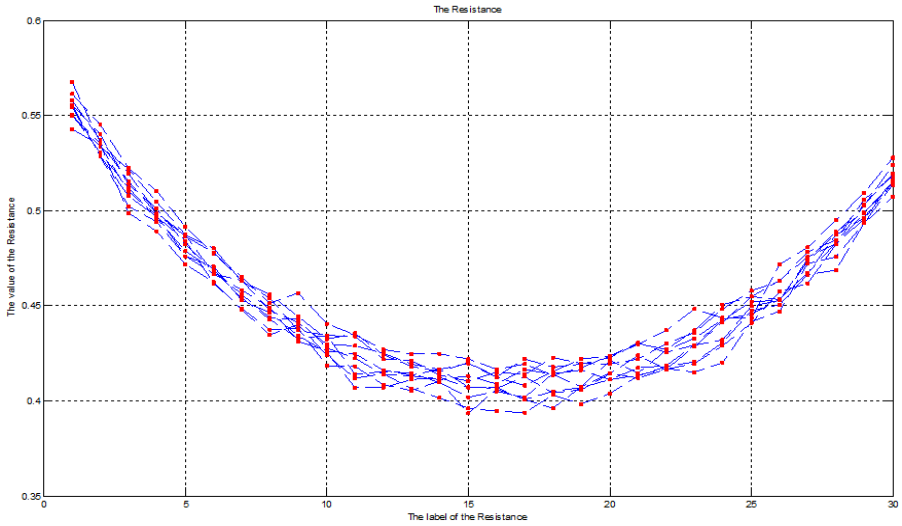

Fig. 5. The row-column resistance with WGN.

In our study, it is assumed that the maximum deformation of electrodes on the row-wire of the upper surface doesn't exceed 20 % of the sensor's height. In the simulation, the size of the flexible tactile sensor is 20 mm×18 mm×5 mm, and the electrodes array scale of tactile sensor is 8×6_3×18.

2.4. Gaussian Noise and White Gaussian Noise

A noise whose probability density function obeys Gauss distribution (normal distribution) is called Gauss noise. If a noise, its amplitude distribution obeys Gauss distribution, and its power spectrum density is uniform distribution, it is called the White Gauss Noise (WGN). The second order moments of WGN are not related to each other, and the first order moments are constants, they refer to the correlation of signal in time. There is no correlation between any two samples of white noise. Gaussian noise is random noise. The one-dimensional probability density function of Gaussian noise can be expressed as a mathematical expression

$$p(x) = \frac{1}{\sqrt{2\pi}\sigma} e^{-\frac{(x-\mu)^2}{2\sigma^2}}, \tag{8}$$

where μ is mean value, σ^2 is variance. Fig. 6 is the density function of normal distribution. When μ is 0, and σ^2 is 1, it is called standard normal distribution.

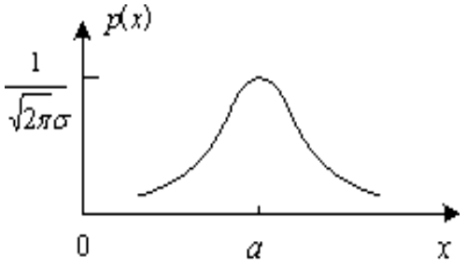

Fig. 6. The density function of normal distribution.

From Fig. 6, it is known that in ($-\infty$, μ), p(x) is monotonically decreased, while in (μ, $+\infty$), p(x) is monotonically increased. μ is the distribution center, σ shows the concentration degree. With different μ, the graphic is left or right shift. If σ is decreased, the graphic of p(x) would be higher and narrower.

The WGN involves two aspects of noise that are the probability density function of normal distribution and the uniformity of power spectral density function. The power spectral density function is defined as:

$$p_n(\omega) = \frac{n_0}{2}, -\infty < \omega < +\infty, \tag{9}$$

n_0 is a constant, its unit is W/Hz.

In the theoretical analysis of communication system, especially when analyzing and computing the anti-noise performance of the system, it is often assumed that the channel noise is the WGN. There are two reasons for us to choose WGN, the first is that it can be described by some specific mathematical expressions, which make analysis and compute easier. The second reason is that it reflects the additive noise in real channel and represents the feature of channel noise.

In the simulation, the noise added to the tactile sensor model is the WGN. Different WGNs are put into the tactile sensor system purposely to simulate the real situation of the tactile sensor and to verify the performance of RBFNN.

3. Improvement of the Radius Basis Function Neural Network

A standard Radius Basis Function Neural Network (RBFNN) has three layers. Firstly, is the input layer, which consists of m0 nodes. Secondly, is the hidden layer, which consists of the computation unit, and the number of the hidden unit is the same as the size of the training sample. Each unit can be described by a radial basis function (RBF)

$$\varphi_j(X) = \varphi(\| X - X_j \|), j = 1, 2, ..., N, \tag{10}$$

X_j defines the center of the RBF, and the vector X is the input signal of the input layer. In this paper, we choose Gaussian function as the RBF

$$\begin{aligned} \varphi_j(X) &= \varphi(\| X - X_j \|) \\ &= \exp(-\frac{1}{2\sigma_j^2} \| X - X_j \|^2), j = 1, 2, ..., N \end{aligned}, \tag{11}$$

σ_j is the width of the j-th Gaussian function with center X_j. Unlike a multilayer perceptron, there are no weights between input nodes and hidden units. Thirdly, is the output layer, without loss of generality, we have purposely chosen a single output unit to simplify the state.

The RBFNN executes a nonlinear mapping from the input space to the hidden space, and a linear mapping from the hidden space to the output space. In an overall fashion, the RBFNN represents a mapping from the m_0-dimensional input space to a one-dimensional output space, which can be written as

$$s: \Re^{m_0} \to \Re^1 \tag{12}$$

The mapping S is viewed as the hypersurface $\Gamma \subset \Re^{m_0+1}$. The hypersurface Γ is a multidimensional plot of the output space as a function of the input space. In practical application, the hypersurface Γ is usually unknown and the training samples are often polluted by a lot of noise.

The learning process includes two phases [16], which are training phase and generalization phase. The training phase is composed of the optimization of a fitting process for the hypersurface Γ, which performing on the known data to the network in form of input-output samples. The task of the generalization phase is to interpolate between the data points. The interpolation is performed along the constrained surface produced by the fitting process of the optimum approximation for the real surface Γ.

This paper uses the RBFNN to solve a high-dimensional and nonlinear interpolation problem. The interpolation problem, in a strict sense, can be described as follows:

Given a set of N different points $\{X_i \in \Re^{m_0} \mid i = 1,2,...,N\}$ and a corresponding set of N real numbers $\{d_i \in \Re^1 \mid i = 1,2,...,N\}$. So the RBF network should to find a special function $F: \Re^N \to \Re^1$ to satisfy the interpolation condition:

$$F(X_i) = d_i, i = 1,2,...,N \tag{13}$$

In this paper, RBF technique should choose a function F with the following form

$$F(X) = \sum_{i=1}^{N} \omega_i \varphi(\| X - X_i \|), i = 1,2,...,N, \tag{14}$$

where $\{\varphi(\| X - X_i \|), i = 1,2,...,N\}$ is the set of N arbitrary functions, which are called radial basis functions.

Inserting the interpolation conditions of Eq. (13) into Eq. (14), we obtain a set of equations for the unknown weights of $\{\omega_i\}$ given by

$$\begin{bmatrix} \varphi_{11} & \varphi_{12} & \cdots & \varphi_{1N} \\ \varphi_{21} & \varphi_{22} & \cdots & \varphi_{2N} \\ \vdots & \vdots & \vdots & \vdots \\ \varphi_{N1} & \varphi_{N2} & \cdots & \varphi_{NN} \end{bmatrix} \begin{bmatrix} \omega_1 \\ \omega_2 \\ \vdots \\ \omega_N \end{bmatrix} = \begin{bmatrix} d_1 \\ d_2 \\ \vdots \\ d_N \end{bmatrix} \tag{15}$$

where $\varphi_{ij}(X) = \varphi(\| X_i - X_j \|), i, j = 1,2,...,N$, set $\phi = \{\varphi_{ij}\}_{i,j=1}^{N}$, $W = [\omega_1 \ \omega_2 \ \cdots \ \omega_N]^T$ and $d = [d_1 \ d_2 \ \cdots \ d_N]^T$, we may rewrite Eq. (15) in a new form

$$\phi W = d \tag{16}$$

The N-by-1 vectors ***W*** and ***d*** represent the linear weight vector and desired response vector, respectively. We call matrix ϕ the interpolation matrix. Assuming that ϕ is nonsingular, which mean that the inverse matrix ϕ^{-1} exists. So ***W*** could be solved by Eq. (17).

$$W = \phi^{-1} d \tag{17}$$

For the radial basis functions listed in Eq. (11) to be nonsingular, the input data {X_i, i=1, 2, …, N} must be different. This is all that is required for nonsingularity of the interpolation matrix ϕ. In our experiment for the tactile sensor, all the input data are different, which ensure that interpolation matrix ϕ is nonsingularity, and the weights matrix ***W*** can be solved correctly.

In practical, it is found that training samples $\{X_i, d_i\}_{i=1}^{N}$ are usually contaminated with noise. Unfortunately, the use of interpolation based on noisy data could lead to misleading results. Hence we need a different approach to design and improve the RBF network. There is another practical issue that needs attention: Having a hidden layer of the same size as the input sample could be wasteful of computational resources, especially when dealing with large training samples. There is redundancy of neurons in the hidden layer when they are chosen in accordance with Eq. (11) by virtue of the redundancy that may inherently exist in the training sample. In this situation, it is better to make the size of the hidden layer less than the size of the training samples, as shown in Fig. 7.

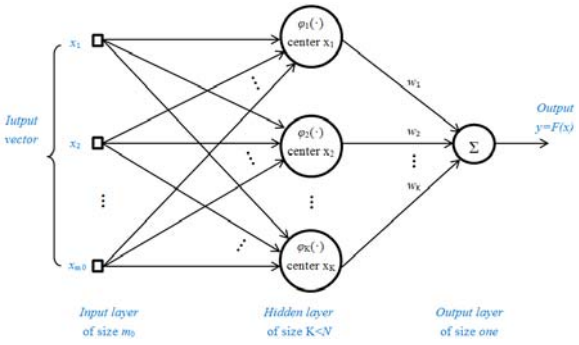

Fig. 7. Structure of the modified RBF network. K is the size of hidden layer that is less than N, N is the size of training samples.

Moreover, the approximating function realized by the modified RBF structure has the mathematical form:

$$F(X) = \sum_{j=1}^{K} \omega_j \varphi(\| X - X_j \|), j = 1,2,...,K, \tag{18}$$

where each hidden nodes is described by the RBF, and K is smaller than N.

In this paper, the learning procedure for the improved RBFNN is hybrid. First, the K-means algorithm is used to train the hidden layer; Second, the recursive least-squares (RLS) algorithm is performed to train the output layer. In this hybrid learning procedure, the size of the hidden layer is

determined by the proposed number of clusters, K; The cluster mean, computed by the K-means algorithm working on the unlabeled sample $\{X_i\}_{i=1}^{N}$ of input vectors, and determines the center X_j in the Gaussian function $\varphi(\bullet, X_j)$ assigned to the hidden unit. The vector

$$\phi(X_j) = \begin{bmatrix} \varphi(X_i, \mu_1) \\ \varphi(X_i, \mu_2) \\ \vdots \\ \varphi(X_i, \mu_K) \end{bmatrix}, \quad (19)$$

denotes the outputs of the K units in the hidden layer. Thus, so far as the supervised training process of the output layer is concerned, the training sample for the output layer can be defined by $\{\phi(X_i), d_i\}_{i=1}^{N}$, where $\boldsymbol{d_i}$ is the desired output of the RBFNN for input $\boldsymbol{X_i}$. This training process is executed by the RLS algorithm. Once the network training is completed, the whole RBF network can be tested by the testing samples that not seen before.

In this paper, the input point for the RBFNN is an 18-dimensional vector of the 3-d deformation for 6 electrodes on a row-wire of the tactile sensor, the desired output is an 18-d vector of the row-column resistance with WGN. The RBFNN is applied
to mapping the relationship between row-column resistance with WGN and 3-d deformation.

4. Decoupling Results of the Tactile Sensor with White Gaussian Noise

In this paper, we modify the traditional RBFNN described in Sec. 3. The hidden nodes number of the modified RBFNN is less than that of its training samples, and the training and testing samples are added in different White Gaussian Noise (WGN) purposely. In the experiments, the flexible tactile sensor model is applied to 10 %, 5 %, 1 %, 0.5 % WGN, based on the different spread values respectively, to verify the anti-noise ability and robustness of the RBFNN method. The decoupling results for the tactile sensor based on the improved RBFNN are shown in Fig. 8 and Fig. 9. In both the two figures, the blue square represents the initial deformation for the electrodes on the upper layer of the tactile sensor, and the red circle represents the decoupling result correspondingly. The two figures imply that the decoupling results of the 3-d deformation are very good. Especially, Fig. 9 describes the decoupling results of the X-direction and Y-direction for the tactile sensor, where the decoupled deformation in both X-dierction and Y-direction corresponds to that of initial deformation very well. It demonstrates that the RBFNN has good performance of anti-noise and high-dimensional nonlinear mapping ability.

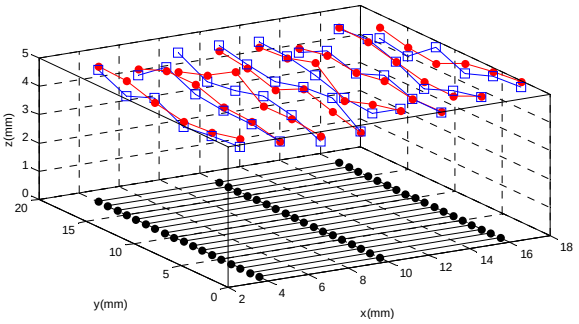

Fig. 8. Decoupling results based on the RBFNN with WGN. The blue square represents the initial deformation for the electrodes on the upper layer of the sensor, and the red circle represents the decoupling deformation correspondingly.

The relative decoupling errors of the deformation based on that RBF network are shown in Table 1. In Table 1, we only list the relative decoupling error of deformation along Z-direction, as all of the decoupling errors of X-direction and Y-direction are nearly zero, which can be proved by Fig. 9. Fig. 9 shows that although there are a lot of noises added into the tactile sensor system, the decoupling results of X-direction and Y-direction are excellent and the decoupled deformation corresponds to the initial deformation very well.

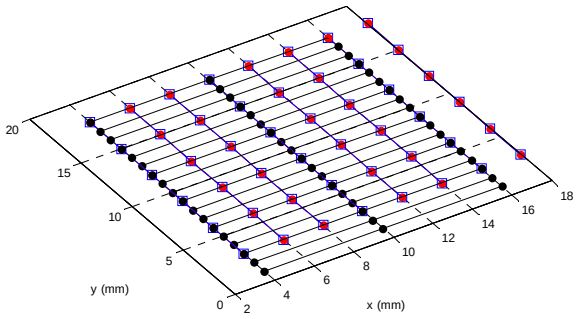

Fig. 9. Decoupling results of X-direction and Y-direction.

From Table 1, it is shown that with the increase of WGN, the decoupling error of deformation increased. It proves that if there are more noises in the training samples, the approximation ability for the RBF network will get weak. So, the network may not accurately approach the mapping between resistances and 3-d deformation involved by WGN.

In the RBFNN, a large spread value would make a wide receptive field of the radial basis neurons and the approximation process is relatively smoother. In this way, the approximation error will be larger and the net needs more hidden neurons. Even if enough hidden neurons are gained, the effect of network may be poor and show “less fitting” phenomenon. On the contrary, if a smaller spread is applied, it may make the receptive field of the radial basis neuron narrower and the net needs less hidden

neurons. If the hidden nodes number increased improperly, the "over fitting" phenomenon may be produced. So, the choice of spread values is very important for the RBFNN. In the experiments, different spread values are used to construct different RBFNN model involved with different WGNs. The results are shown in Table 1.

Table 1. Relative decoupling errors of deformation for the sensor interfered by WGNs.

Spread	Relative decoupling errors of deformation interfered by different WGNs			
	0.5 % WGN	1 % WGN	5 % WGN	10 % WGN
0.1	6.47 %	7.89 %	9.12 %	9.55 %
0.2	7.23 %	9.20 %	9.52 %	9.78 %
0.3	7.77 %	10.23 %	9.78 %	9.81 %
0.4	8.21 %	9.50 %	9.77 %	9.75 %
0.5	8.37 %	9.27 %	9.98 %	9.84 %
0.6	8.80 %	9.70 %	9.98 %	10.56 %
0.7	8.82 %	9.23 %	10.33 %	10.64 %
0.8	8.36 %	9.29 %	10.18 %	10.86 %
0.9	8.89 %	9.42 %	10.06 %	11.23 %
1.0	9.31 %	11.11 %	10.67 %	11.39 %

From Table 1, it can be seen that with the increase of spread values under the same WGN, the relative decoupling errors increases slowly. Under the same condition of troubled by the WGN, the relative decoupling errors of deformation of Z-direction are not so good as that of X-direction and Y-direction, but they are also acceptable, as most of the relative decoupling errors of Z-direction are less than 10 %. All of the experimental results imply that the improved method we proposed has good function in decoupling the 3-d deformation for the flexible tactile sensor interfered by WGN.

5. Conclusions

This paper presents an efficient method to imitate the real situation of the flexible tactile sensor in practical application. The different white Gaussian noises are put into the sensor model, and the modified RBFNN is applied to approximate the mapping relationship between 3-d deformation and resistance for the sensor troubled by noise. All of the decoupling results indicate that the improved RBFNN has good performance in decoupling high-dimensional nonlinear mapping problems and anti-noise ability.

In this paper, many factors in the model are still neglected. For example, the material property of the conductive rubber is very complex and the viscoelastic and some other characteristics of the conductive rubber are not considered. In the future, we will improve the model of the flexible tactile sensor by considering the actual properties of the tactile sensor and explore new decoupling algorithms.

Acknowledgements

The paper is supported by NSF of Anhui (No. 1408085QF123), Outstanding Young Talent Foundation Project in Colleges and Universities of Anhui (Nos. 2012SQRL130, 2012SQRL129), and NSFC (Nos. 61175070, 61273324, 61201076, and 61301060).

References

[1]. Sumer Bilsay, Aksak Burak, Ssahin Korhan, *et al.*, Piezoelectric Polymer Fiber Arrays for Tactile Sensing Applications, *Sensor Letter*s, 9, 2, 2011, pp. 457-463.

[2]. Pirozzi S., Multi-Point Force Sensor Based on Crossed Optical Fiber, *Sensors and Actuators A: Physical*, 183, August 2012, pp. 1-10.

[3]. Stefan C. B. Mannsfeld, Zhenan Bao, *et al.,* Highly Sensitive Flexible Pressure sensors with Microstructured Rubber Dielectric Layers, *Nature Materials*, 9, Oct. 2010, pp. 859-864.

[4]. Zhou Zhijian, Wong Man, Rufer L., The Design, Fabrication and Characterization of a Piezoresistive Tactile Sensor for Fingerprint Sensing, in *Proceedings of the IEEE Conference on Sensors*, Kona, Hi, 1-4 Nov., 2010, pp. 2589-2592.

[5]. H. B. Muhammad, C. Recchiuto, C. M. Oddo, *et al.*, A capacitive Tactile Sensor Array for Surface Texture Discrimination, *Microelectronic Engineering*, 88, 8, 2011, pp. 1811-1813.

[6]. S. H. Li, Y. J. Ge, *et al.*, Mechanism and Simulation Research on a 3D Flexible Tactile Sensor Array Based on Conductive Rubber, *Chinese Journal of Sensors and Actuators*, 26, 4, 2013, pp. 476-480.

[7]. Fei Xu, Simulation Research of a Novel Three-Dimensional Force Flexible Tactile Sensor Based on Force-Sensitive Conductive Rubber, *Chinese Journal of Sensors and Actuators*, 25, 3, 2012, pp. 359-4364.

[8]. Tao Liu, Yoshio Inoue, Kyoko Shibata, Design of Low-cost Tactile Force Sensor for 3D Force Scan, *in Proceedings of the IEEE Conference on Sensors,* Lecce, Italy, 26-29 Oct. 2008, pp. 1513-1516.

[9]. J. H. Kim, J. I. Lee, *et al.*, Design of Flexible Tactile Sensor Based on Three-Component Force and Its Fabrication, in *Proceedings of the Conference on Robotics and Automation (ICRA'05)*, 18-22 April 2005, pp. 2578 -2581.

[10]. Xuekun Zhuang, Yunjian Ge, *et al.*, Radical Basis Function Neural Network for A Novel Tactile Sensor Design, in *Proceedings of the IEEE International Conference on Information and Automation (ICIA'12)*, Shenyang, China, June 2012, pp. 926-931.

[11]. J. X. Ding, Y. J. Ge, Comparison of Application between Evolutionary Algorithm and Algorithm Based on Homotopy Theory for Multidimensional Tactile Array Sensor Decoupling, *Artificial Intelligence and Pattern Recognition*, 25, 6, 2012, pp. 375-381.

[12]. F. L. Wang, X. K. Zhuang, *et al.*, The Study of Decoupling Methods for a Novel Tactile Sensor Based on BP Neural Network, *Sensors & Transducers*, Vol. 150, Issue 3, March 2013, pp. 18-26.

[13]. F. L. Wang, Feng Shuang, *et al.*, Decoupling Research of a Three-dimensional Force Tactile

Sensor Based on Radical Basis Function Neural Network, *Sensors & Transducers*, Vol. 159, Issue 11, 2013, pp. 289-298.

[14]. Y. Huang, B. Xiang, *et al.*, Conductive mechanism research based on pressure-sensitive conductive composite material for flexible tactile sensing, in *Proceedings of International Conference on Information and Automation (ICIA'08)*, China, 20-23 June 2008, pp. 1614-1619.

[15]. F. Xu, Y. J. Ge, *et al.*, The Design of a Novel Flexible Tactile Sensor Based on Pressure-conductive Rubber, *Sensors & Transducers*, Vol. 124, Issue 1, 2011, pp. 19-29.

[16]. Simon Haykin, Neural Networks and Learning Machines (3rd Edition), *Prentice Hall*, 2008.